Chinese Journal of
POLYMER SCIENCE

RESEARCH ARTICLE

https://doi.org/10.1007/s10118-024-3113-9
Chinese J. Polym. Sci.

Self-healable and Robust Film Based on Electroactive Polymer Brush as Electrode for Flexible Supercapacitor

Maria P. Sokolova*, Vitaly K. Vorobiov, Nikolay N. Smirnov, Ivan S. Kuryndin, Natalya V. Bobrova, and Michael A. Smirnov*

Institute of Macromolecular Compounds, Russian Academy of Sciences, Bolshoy pr. 31, Saint Petersburg 199004, Russia

Electronic Supplementary Information

Abstract The aim of this study was to develop self-healable and robust electroconductive film based on polyaniline copolymer for application as electrode in flexible supercapacitor. For this purpose, the electroconductive polymer brushes (EPB) was elaborated. The synthesis of EPB is based on graft polymerizations of acrylamide (AAm) on poly(vinyl alcohol) (PVA) with formation of PVA-PAAm polymer brush and subsequent graft copolymerization of aniline and *p*-phenylenediamine on PVA-PAAm resulting in formation of EPB with electroconducting copoly(aniline-*co*-*p*-phenylenediamine) (PAPhDA). It was found that the ratio between PVA and PAAm at the first stage greatly influence the electrochemical performance of the EPBs. Electroconducting films were prepared by casting of EPB solution with subsequent drying. Investigation of electrical current distribution through the film with AFM reveal more uniform distribution of PAPhDA in EPB in comparison with reference PVA-PAPhDA and PAAm-PAPhDA samples. It was demonstrated that mechanical characteristics and electrical conductivity values of films restore at large extent after curring and self-healing under optimal relative humidity level (58%). The flexile supercapacitor cell with EPB film electrodes demonstrate specific capacitance 602 mF·cm^{-2} at the current density of 1 mA·cm^{-2} and retention 94% of initial capacitance after 5000 charge/discharge cycles.

Keywords Polymer brush; Polyaniline; Flexible supercapacitor; Self-healing; Electroconducting film

Citation: Sokolova, M. P.; Vorobiov, V. K.; Smirnov, N. N.; Kuryndin, I. S.; Bobrova, N. V.; Smirnov, M. A. Self-healable and robust film based on electroactive polymer brush as electrode for flexible supercapacitor. *Chinese J. Polym. Sci.* https://doi.org/10.1007/s10118-024-3113-9

INTRODUCTION

Electroconducting polymers attract a lot of attention[1] because of their low toxicity, easy synthesis and electroactivity. They are intensively studied in recent years for elaboration of energy storage devices,[2] electrochemical sensors,[3] coatings,[4] water purification,[5] packaging films with antioxidant and antibacterial activity,[6] nerve regeneration[7] and actuators.[8] The increasing interest toward wearable electronics[9] result in intensive elaboration of flexible supercapacitors[10–12] based on electroconductive polymer electrodes demonstrating morphology and structure beneficial for high capacitance, namely accessibility of internal electrode volume for electrolyte due to porosity[13] or hydrogel nature.[14,15] The desired morphology can be achieved by self-organization of electroconductive polymer during synthesis,[16] by applying electrospinning technique,[17,18] or by using of a template.[19] One of the remaining problems of electroactive polyaniline-based hydrogels is bad mechanical properties.[20]

Poor mechanical properties of pure conducting polymers lead to the intensive elaboration of composite materials containing non-conductive supporting ones.[21,22] The main problem in this field is poor compatibility of conducting polymers with most of industrial polymers. To fit this the following approaches are intensively studied: (i) mechanical fixing of conducting polymer inside porous matrix,[23] (ii) chemical grafting of conductive chains to the matrix polymer[24] or chemical routs toward increasing hydrophilicity of support[25] were proposed. Due to ability of the most common oxidizer for polyaniline (PANI) synthesis (ammonium peroxydisulphate) to generate radicals on the backbones of supporting macromolecules it is possible to expect grafting of PANI chains during their formation. It was demonstrated[26] that the grafting of PANI chains onto poly(glycidyl methacrylate-*alt*-maleic anhydride) using "grafting on" improve solubility in polar organic solvents, while grafting to the polyacrylamide (PAAm) increase compatibility with water.[27]

Poly(vinyl alcohol) (PVA) is industrial and cheap polymer that is usually used for preparation of flexible materials with electroconducting polymers because of its easy processing, low toxicity and low cost. Composites PVA/conducting polymer are elaborated during last decades for application as stretchable electronic skins and intelligent robotic systems,[28]

* Corresponding authors, E-mail: pmarip@mail.ru (M.P.S.)
E-mail: smirnov_michael@mail.ru (M.A.S.)

Received December 10, 2023; Accepted March 27, 2024; Published online May 10, 2024

for electromagnetic shielding, batteries, supercapacitors.[29] The benefits of combining of PVA with PANI is beneficial for preparation of strong, elastic, biocompatible and electrically conductive materials. However, these polymers have low compatibility[30] and there are no reported approaches for grafting of electroconductive polymer to PVA backbone. Additionally, the desire to have materials with self-healing properties similar to human skin motivates scientists to develop materials with dynamic hydrogen or coordination bonds.[31,32] The PVA is one of the often used polymer for self-healable materials due to its ability to form cooperative hydrogen bonds.[33]

Thus, in this work we report for the first time the strategy toward preparation of branched macromolecules, containing electroconductive end chains grafted to the PVA-electroconductive polymer brushes (EPB). For this purpose, the PVA-PAAm polymer brushes were synthesized according to known procedure.[34] Synthesis of copoly(aniline-*co*-*p*-phenylenediamine) (PAPhDA) was conducted in the presence of PVA-PAAm polymer brush that allow grafting of conducting polymer to the PAAm side chains according to scheme reported earlier.[35] It was proposed that by combination of these reactions it will be possible to prepare polymer flexible and self-healable electroactive electroconductive materials with high strength, that can act as electrodes in electrochemical energy storage devices.

EXPERIMENTAL

Materials

Acrylamide (AAm, purity ≥98%), PVA (M_w=1.25×10^5), aniline hydrochloride (≥99.0%) and *p*-phenylenediamine (≥97.5%) were purchased from Sigma Aldrich (Czech Republic). Methanol (≥ 99.5%), 38 wt% hydrochloric acid (HCl), 64 wt% nitric acid (HNO_3), 98 wt% sulfuric acid H_2SO_4 were acquired in Vekton (Russia). Cerium(IV) ammonium nitrate (CAN, ≥99%) was procured from Acros Organics (Belgium), while ammonium persulfate (APS, ≥99%) and paraphenylenediamine (pPhDA, ≥99%) from Neva Reactive (Russia). All reagents were used as received without purification. Dialysis membrane bag (*d*=25 mm) OrDial D14 with a pore size of 12–14 kDa was purchased in Orange Scientific (Belgium).

Synthesis of PVA-PAAm (PB)

The specific quantities of each reagent used can be found in Table 1. Weighed PVA powder was dissolved in 25 mL of distilled water at 80 °C under vigorous stirring. The solution was cooled down to room temperature and AAm was added. Afterward, a 3 mL of 0.1 mol/L cerium(IV) ammonium nitrate solution in 1 mol/L HNO_3 was added to the mixture. The reaction mass was then thoroughly mixed for one hour and left to proceed overnight. The resulting viscous PVA-PAAm copolymer solution was then precipitated into methanol and dried under vacuum. The copolymers obtained are referred as PB-1, PB-2 and PB-3.

Table 1 The initial ratio of the components of the obtained copolymers.

Sample	PVA (g)	AAm (g)	Initial ratio (molar)
PB-1	3.75	3.75	1:0.62
PB-2	3.75	1.88	1:0.31
PB-3	1.88	3.75	0.81:1

Synthesis of PVA-PAPhDA

PVA (1.06 g) was dissolved in water (14 mL) at 70 °C. Then, aniline hydrochloride (0.518 g), *p*-phenylenediamine (0.0186 g), concentrated hydrochloric acid (1.376 mL) and ammonium persulfate (0.953 g) (pre-dissolved in 2 mL of distilled water) were added. The reaction was conducted at room temperature for 1.5 h with stirring.

Synthesis of PAAm-PAPhDA

PAAm (0.53 g) was dissolved in water (7 mL) at room temperature. Then, aniline hydrochloride (0.259 g), *p*-phenylenediamine (0.0093 g), concentrated hydrochloric acid (0.688 mL) and ammonium persulfate (0.476 g) (pre-dissolved in 1 mL of distilled water) were added. The reaction was conducted at room temperature for 1.5 h with stirring.

Synthesis of PVA-PAAm-PAPhDA (EPB)

The EPB was synthesized as follows (see Fig. 1). PVA-PAAm (1.06 g) was dissolved in water (14 mL) at 80 °C. Then, aniline hydrochloride (0.5184 g), *p*-phenylenediamine (0.0186 g), concentrated hydrochloric acid (1.376 mL) and ammonium persulfate (0.953 g) (pre-dissolved in 2 mL of distilled water) were added to the reaction mass. The reaction was conducted at 0 °C for 1.5 h with stirring. Afterward, the mixture was diluted with 100 mL of distilled water and left for two days. A transparent green supernatant fraction, containing dissolved PVA-PAAm-PAPhDA copolymer was decanted and used for further experiments.

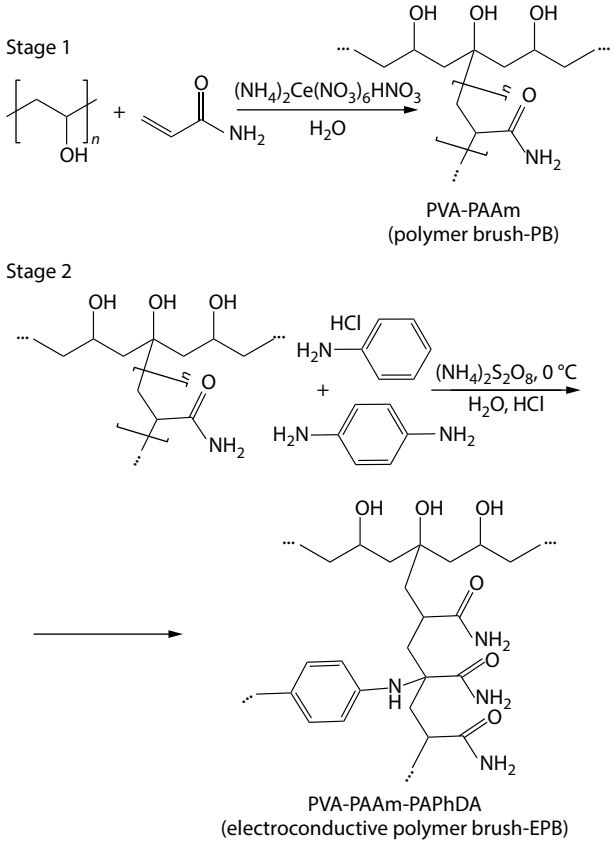

Fig. 1 Scheme of synthesis of water-soluble copolymer.

https://doi.org/10.1007/s10118-024-3113-9

Preparation of Films

The PVA-PAPhDA, PAAm-PAPhDA and PVA-PAAm-PAPhDA solutions cast on a Petri dishes and dried under ambient conditions until it reached a constant weight. The self-supported films were obtained.

Preparation of Chitosan Containing Deep Eutectic Solvent (DES) Gel Electrolyte

Pseudo-solid polymer electrolyte films with a DES content of 90 wt% were prepared using the method described earlier.[36] The DES comprised choline chloride and lactic acid with a molar ratio of 1:2, respectively. Chitosan (CS) and DES constituents were dissolved in distilled water to a total concentration of 2 wt%. Self-supported films were prepared by casting solution on Petri dishes.

Characterization of Chemical Structure and Morphology

^{13}C-NMR measurements

^{13}C-NMR spectra were measured on an AVANCE II-500 WB NMR spectrometer (Bruker, USA) operating at resonance frequency of 125.8 MHz in solid state. The samples were preliminarily ground into powder.

Fourier transform infrared (FTIR) measurements

FTIR spectra were obtained using IRAffinity-1S spectrometer (Shimadzu, Japan) in the range 4000–400 cm^{-1} for copolymers dispersed in KBr pellets in transmission mode with a resolution of 4 cm^{-1} and 50 scans per sample.

UV-spectroscopy measurements

UV-spectroscopy was conducted for aqueous solution of samples using SF-2000 spectrophotometer (OKB "Spectr", Russia) and quartz cuvettes with 1 cm optical length.

Scanning electron (SEM) and atomic force (AFM) microscopy

The morphology of EPB films and cross-sections were studied with a Tescan scanning electron microscope Vega III (Tescan, Czech Republic) at 5 kV. For observation of the cross-sections samples were cooled with liquid nitrogen and then fractured. Scanning Probe Microscope BRUKER Multimode 8 (USA) operating in PeakForce TUNA Tapping mode was used to simultaneously obtain images of surface topography and electrical current. AFM images were obtained using conductive AFM probes SCM-PIT (f=48 kHz, k=0.95 N·m^{-1}, r≈22 nm) providing the force setpoint of 10 nN.

Measurements of Physico-Chemical Properties

Water sorption measurements

The water sorption isotherms of the EPB films were measured gravimetrically using an AP225WD semi-micro analytical balance (Shimadzu, Japan). The samples were dried in a vacuum at 50 °C and then placed in desiccators containing the saturated water solutions of H_2SO_4, KOH, $CaCl_2$, $MnCl_2$, NaCl and K_2SO_4 with constant relative humidity (RH) levels of 2%, 15%, 35%, 57%, 75% and 98%, respectively.

When the constant weight was reached the equilibrium water sorption (a, g/g) was calculated as:

$$a = \frac{w_2 - w_1}{w_1} \quad (1)$$

where w_1 and w_2 are the initial (dry) und final (saturated with water) weights, respectively.

Mechanical and self-healing properties

The mechanical characteristics of the initial and self-healed films were determined at room temperature (25±2 °C) using UMIV-3 (Ivanovo, Russia) mechanical testing machine operating in the uniaxial tension mode (speed 5 mm/min). The films with thickness of 240±30 μm were cut into strips with the length of 20 and a width of 2 mm. Determination of Young's modulus (E), ultimate strength (σ_b), and elongation at break (ε_b) were performed according to ASTM D882.

Self-healing properties of films were also evaluated by macroscopic observation. A long strip film (50 × 10 mm) was prepared. Then, the film was cut and repaired at room temperature (25±2 °C) by 5 min pressing with fingers and subsequent healing by 1 h. After that, the healed film was loaded with 200 g to test its strength.

Electrochemical measurements in solution

The redox properties of the EPB in solution were studied using cyclic voltamperometry (CVA). Measurements were made in a three-electrode cell in the 1 mol/L aqueous H_2SO_4 as the electrolyte. The working (Pt-wire) and reference (Ag/AgCl) electrodes were put into the dialysis bag (pore size 12−14 kDa) filled with the EPB. This bag was placed in the vessel filed with blank electrolyte and containing current electrode (Pt-wire). The CVA was performed at 1 mV/s scanning rate. The scheme of experiment is given in Fig. S1 (in the electronic supplementary information, ESI).

Electrical conductivity of films

The electrical conductivity (σ) of EPB film before and after self-healing was measured using the four-probe method. Four flat graphite foil contacts (1 mm wide and 5 mm gap) placed on a non-conductive plexiglass plate was used. To determine the sheet resistance (R_s) of the samples, the voltammetric response was analyzed using a scan rate of 10 mV/s within a voltage range of −100 mV to 100 mV. The R_s values were calculated from the slope of the curve. The electrical conductivity was then calculated as:

$$\sigma = \frac{l}{R_s \cdot h} \quad (2)$$

where l represents the length between inner probes (cm), and h is the cross-sectional area of the sample (cm^2).

Electrochemical performance of supercapacitor

Taking into account the increased interest toward flexible biopolymer-based electrolytes, a chitosan-based film comprising 90 wt% of DES reported earlier[36] was utilized as a solid polymer electrolyte in a symmetrical supercapacitor cell. It was sandwiched between two PVA-PAAm-PAPhDA films acting as electrode materials with an area of 1.2 cm^2 and thickness of 240±30 μm. Graphite foil was used as a current collector. The electrochemical performance of the two-electrode supercapacitor was investigated with galvanostatic charge-discharge (GCD), CVA and impedance spectroscopy measurements using a P40-X galvanostat-potentiostat equipped with FRA-24M module (Elins, Moscow, Russia). Specific capacitance (C_s) normalized to the electrode area was determined from the GCD data at various current densities using the equation:

$$C_s = \frac{It}{(U_2 - U_1 - IR_{drop})S} \quad (3)$$

where I is the discharge current (A), t is the discharge time (s),

($U_2 - U_1$) is the working potential window of the supercapacitor (V), IR_{drop} is the voltage drop (V) and S represents the area of the electrode (cm^2). The mass normalized specific capacitance was calculated by the same equation with replacing of S with mass of PAPhDA in electrodes.

The areal energy density (E_s, $\mu W \cdot h \cdot cm^{-2}$) and power density ($P_s$, $mW \cdot cm^{-2}$) values were calculated using the following equations:

$$E_s = \frac{0.5(U_2 - U_1 - IR_{drop})^2 C_s}{3600} \quad (4)$$

$$P_s = \frac{E_s}{t} \cdot 3600 \quad (5)$$

Redox behavior of the electrodes was studied by CVA test at the scan rate of 10 $mV \cdot s^{-1}$ in potential range of 0–600 mV. Cycling stability of supercapacitor was assessed by subjecting it to 5000 GCD cycles at a current density of 2 $mA \cdot cm^{-2}$. Electrochemical impedance spectroscopy measurements were conducted in a frequency range of 10 mHz–0.3 MHz at open circuit potential with 20 mV amplitude.

RESULTS AND DISCUSSION

Chemical Structure and Electrochemical Activity of EPB

During the preliminary study, the three types of PVA-PAAm copolymers (PB) were synthesized with different amounts of PAAm grafted onto PVA (see Table 1). The ^{13}C-NMR spectra for the initial PVA (Fig. 2) demonstrates typical for this polymer methylene carbon signals at 45 ppm, along with methine ones resonance lines at 65, 71 and 77 ppm, corresponding to syndiotactic, heterotactic and isotactic triads.[37] Additionally, weaker signals at 22 and 172 ppm can be attributed to the methyl and carbonyl groups of the vinyl acetate residual units in PVA[38] In the case of PB samples, an additional signal at 180 ppm corresponding to the carbon of the amide group of PAAm is observed. A shoulder peak centered at 35 ppm is related to the methylene carbons of PAAm. These peaks become more pronounced as the PAAm content increases (from PB-1 to PB-3). The changing of relative intensity of peaks near 70 ppm allow to propose that the corresponding carbons are involved in the grafting of PAAm as starting points (Fig. 1).[39] Using the ratio of

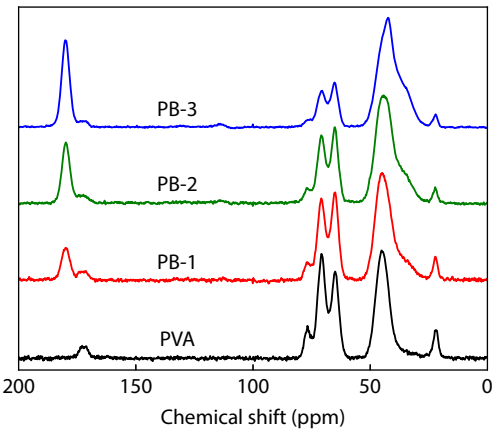

Fig. 2 ^{13}C-NMR spectra for PVA-PAAm polymer brushes prepared at different ratios between PVA and AAm monomer.

area of signals centered at 70 m.d. and 180 m.d. It is possible to estimate the molar ratio between monomer units in PVA and PAAm side chain as 1:0.22, 1:0.45 and 1:1.05, for PB-1, PB-2 and PB-3, respectively.

At the second stage, in the presence of the PVA-PAAm copolymer, oxidative copolymerization of aniline and *p*-phenylenediamine was performed. The spectroscopic evidence of PAPhDA grafting to the PAAm and high yield of this reaction in the selected conditions were demonstrated previously.[35] Thus, the amount of electroconductive component inside EPB can be estimated as 30 wt%. The materials prepared on the base of PB-1, PB-2 and PB-3 will be denoted as EPB-1, EPB-2 and EPB-3 during further discussion.

The chemical structure of the obtained EPB was characterized by FTIR and UV-spectroscopy. The typical UV spectra of EPB water solution (Fig. 3a) reveals an absorption band in the 340–450 region that may be due to electron π-π^* transition in benzenoid rings and polaron formation in the PANI chain.[40] Additionally, a broad band near 800 nm is observed, which is attributed to polaron-π^* excitation.[41] The presence of absorption near 400 and 800 nm regions typically indicates the existence of localized and delocalized cation-radical structures, respectively.[42] These structures are typical for the electrically conductive form of PANI. Furthermore, an additional absorption peak at 285 nm corresponds to transitions in aromatic rings containing electron-donating substituents that may be associated with the presence of *p*-phenylenediamine fragments in the PAPhDA chains. Notably, these peaks are not observed in the UV spectrum of the PVA-PAAm solution (Fig. 3a).

The FTIR spectra (Fig. 3b) were measured for individual polymers (PAPhDA, PVA and PAAm) and EPB. Bands of PANI copolymer can be found near 1558 cm^{-1} (C=N and C=C stretching vibration of quinoid ring), 1301 cm^{-1} (C—N stretching of the secondary aromatic amine), 1242 cm^{-1} (C—N^+ stretching) and 875 cm^{-1} (aromatic C—H out-of-plane bending deformation vibrations) as well as shoulders near 1472 cm^{-1} (C—C stretching in benzenoid ring) and 802 cm^{-1} (C—H out-of-plane bending in aromatic ring).[43] This result along with UV spectrum proves incorporation of PAPhDA into the PVA-PAAm PB.

In order to select the most electrochemically active type of EPB, the electrochemical properties of EPB brush solution were checked with CVA using cell (Fig. S1 in ESI) in which the solution of EPB near working and reference electrodes was separated from other volume with dialysis membrane. It was found that (see Fig. 4) the area covered with CVA curve is the maximal for EPB-2 sample (with middle PAAm content), while for others it is not significantly exceeds the curve corresponding for blank solution. It can be attributed to the highest compatibility of EPB with water solution. The possible explanation can be the following taking into account the equivalent amount of PAPhDA in electroconducting polymer brush. At lower PAAm content the density of PAPhDA side chains is higher that decrease the compatibility of material with solvent. While at higher PAAm content the relative amount of not electroactive components (PAAm+PVA) becomes higher that leads to the decreasing of the electrochemical activity. According to this result the EPB-2 sample was selected for

https://doi.org/10.1007/s10118-024-3113-9

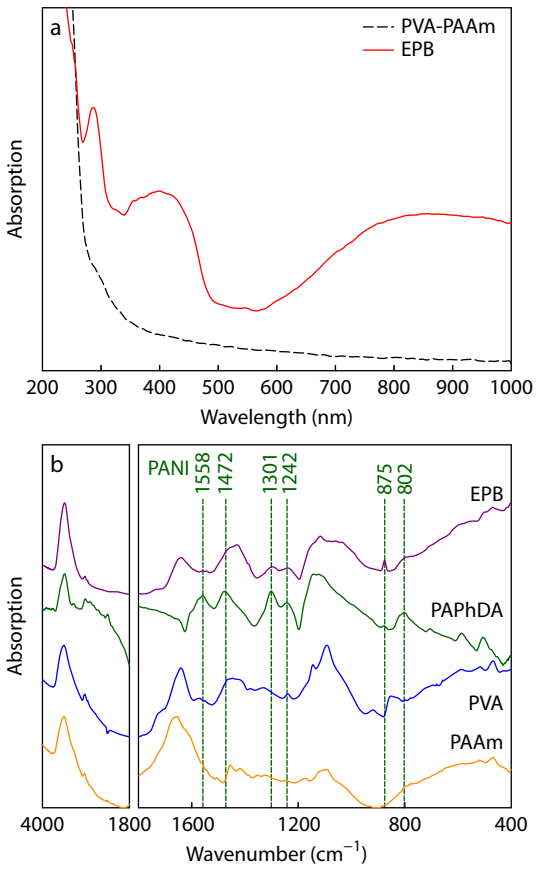

Fig. 3 UV-visible spectra of water solution of PVA-PAAm and EPB (a); FTIR spectra (b) of EPB and corresponding homopolymers (PAPhDA, PVA and PAAm).

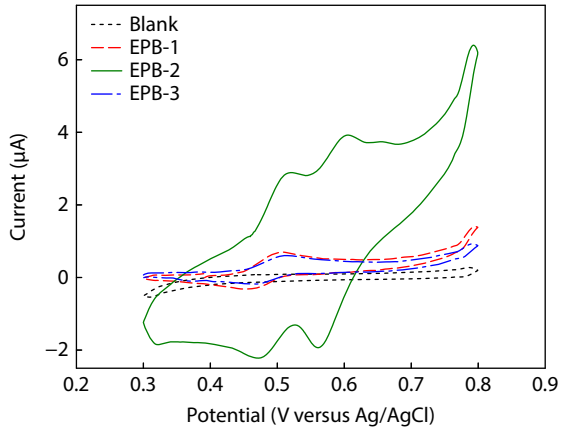

Fig. 4 CVA curves for blank solution (1 mol/L H_2SO_4 in water) and different synthesized EPB.

film preparation and will be denoted as EPB during further discussion.

Study of Morphology and Phase Structure of Films based on EPB using AFM

The internal structure of films prepared on the base of EPB-2 was studied using AFM. In order to evaluate the influence of "double brush" structure on the morphology of films it is interesting to compare results between samples containing only two polymers (PAAm-PAPhDA or PVA-PAPhDA) and EPB. It is seen that surface of PAAm-PAPhDA is free from worm-like objects clearly visible for PVA-PAPhDA (Figs. 5a and 5c, respectively) and are typical for PAPhDA.[44] It can be considered as additional evidence that only in the case of PAAm, the grafting of conducting polymer onto the backbone of carbon-chain one occurs and results in the destruction of the intrinsic morphology of PAPhDA. The morphology of surface of EPB (Fig. 5e) film is closer to the morphology of PAAm-PAPhDA that also demonstrates the suppression of formation of PAPhDA homopolymer intrinsic structure and gives evidence for formation of electroconductive polymer brushes.

For the evaluation of electric properties of materials on nanoscale the maps of electrical current distributions along the surface were obtained. As it is seen from Figs. 5(b) and 5(d), the formation of electroconductive channels with low conductivity between them is typical for the PAAm-based sample. In the case of PVA, currents through surface are significantly lower and the map of currents is smoother (Fig. 5d). This can be explained by the different action of PVA and PAAm during preparation of conducting polymer by *in situ* method. PVA acts as a stabilizer by adsorption on the surface of growing PANI copolymer particles, while PAAm is a backbone for PAPhDA grafting. Thus, for PVA-PAPhDA the electroconducting part is surrounded by PVA, while for PAAm-PAPhDA the electroconducting component is outside of the molecular objects. In the latter case the formation of continuous electroconductive network is easier that is reflected by higher number of bright objects and higher overall current in the case of PAAm-PAPhDA. In the case of EPB (Fig. 5f) the look

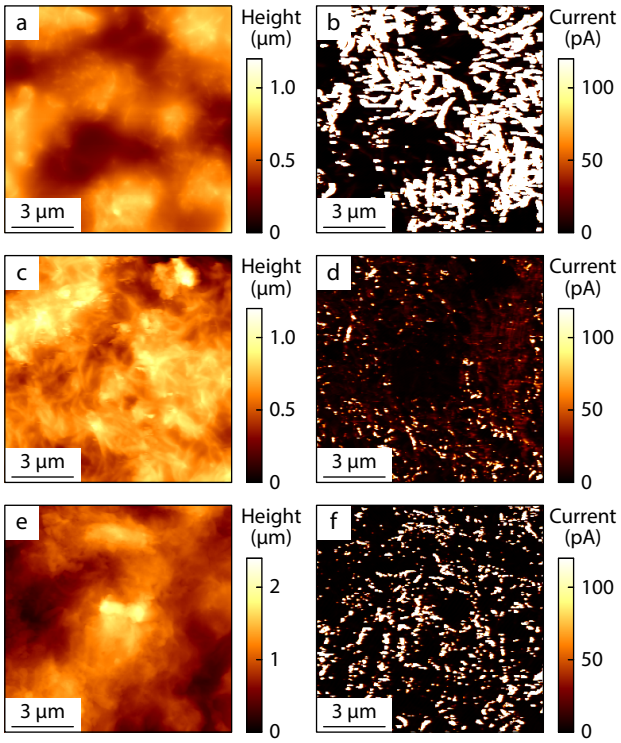

Fig. 5 Surface relief maps (a, c, e) and maps of electric current distribution along the surface (b, d, f) for PAAm-PAPhDA (a, b), PVA-PAPhDA (c, d) and EPB (e, f).

https://doi.org/10.1007/s10118-024-3113-9

of map of electrical currents is closer to the PAAm-PAPhDA (Fig. 5b) however, electroconducting areas are smaller and more uniformly distributed along the surface. This demonstrates the formation of similar continuous electroconductive network with thinner pathways and gives evidence for successful grafting of PAPhDA to PAAm in the case of using PVA-PAAm.

Mechanical Properties, Electroconductivity and Self-healing of EPB

The stress-strain and voltampere curves are given in Figs. 6(a) and 6(b), respectively, while mechanical properties presented in Table 2. It is seen that tensile strength and elongation at break is higher for PVA-PAPhDA in comparison with PAAm-PAPhDA. This can be attributed to the encapsulation of PAPhDA component inside PVA that is not the case for PAAm as it was shown with AFM. The tensile strength and elongation at break for EPB films is closer to the PVA-PAPhDA, while Young's modulus is approximately the same as for PAAm-PAPhDA (see Table 2). The latter fact can be attributed to the formation of hard electroconductive continuous network that influences mechanical properties before 10% of relative elongation. At further elongations this network destroyed and the PVA begin to determine mechanical properties of material. At the relative elongation ε>10%, the course of the curve of the EPB sample is similar to that of the PAAm-PAPhDA sample (Fig. 6a). The changing of the mechanical behavior during stretching is seen as the point at which the slope of mechanical curve is changed. It should be noted that double polymer brush PVA-PAAm (PB) demonstrate the most rigid and fragile behavior than other samples (see Fig. S2 in ESI, Table 2). This is connected with high energy hydrogen bonding between amide groups of PAAm. The lower brittleness and rigidity of materials with PAPhDA demonstrate that interaction between PAAm macromolecules is hampered that is also confirms grafting of conducting polymer to PAAm in the both cases: PAAm-PAPhDA and EPB.

Taking into account that water is a plasticizer for studied materials and thus it influences on macromolecular chain mobility, the study of self-healing was conducted at different relative humidity. For this purpose, the strips (5 × 40 mm) of films prepared from EPB were placed in desiccators over the saturated water solutions of inorganic salts that allow to maintain certain humidity (RH = 2%, 15%, 35%, 57%, 75% and 98%). After saturation during 24 h samples were cut, connect-

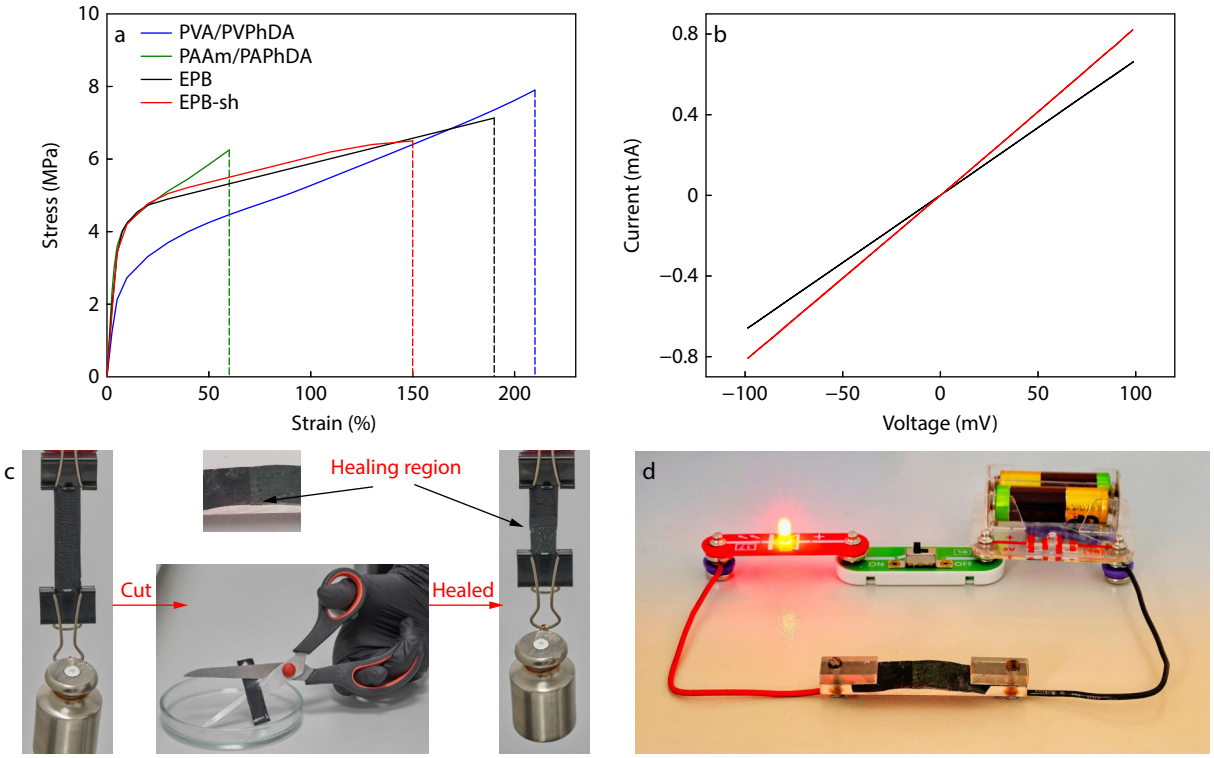

Fig. 6 (a) Stress-strain curves for PVA-PAPhDA, PAAm-PAPhDA, EPB film and self-healed EPB film; (b) Dependences of current on applied voltage for initial (red line) and self-healed EPB film (black line); Photos demonstrating mechanical properties (c) and electroconductive (d) of the self-healed EPB film.

Table 2 The mechanical properties of samples.

Sample	Tensile strength (δ, MPa)	Ultimate elongation (ε, %)	Young's modulus (E, MPa)
PVA-PAAm	93±10	3.1±0.2	3800±400
PVA-PAPhDA	7.9±1.0	205±20.8	45±5.0
PAAm-PAPhDA	5.0±0.6	60±7.3	72±7.5
EPB	7.3±0.8	183±19.5	68±6.3
EPB-sh	6.2±0.7	145±15.2	65±5.8

https://doi.org/10.1007/s10118-024-3113-9

ed with 5 mm of overlapping and put back to the desiccator for 1 h. Then films were taken out of desiccators and their mechanical properties were tested. It was found that at humidities 2, and 15 self-healing does not proceed. At RH=35 self-healing proceeds, but it takes 24 h to achieve minimum mechanical stability allowing to handle self-healed film, while at RH=57% films were self-healed after 1 h and it was enough to perform mechanical experiments (the corresponding sample will be denoted as EPB-sh). At RH=75% and 98% films self-healed but, connection was weak—the integrity of films preserved only without mechanical load. The stress-strain curves of the EPB-s sample after the self-healing and values of mechanical properties for it are given in Fig. 6(a) and Table 2, respectively. The degree of recovery of tensile strength, ultimate elongation and Young's modulus is 85%, 79% and 96 %, respectively. The mechanical properties of reported self-healed electroconducting materials are in the region of 50%–100% recovery of initial ones.[1] Thus, in our case the recovery is closer to the upper border. Moreover, it was noticed that the rupture of self-healed film takes place outside the binding zone.

To further demonstrate the superior mechanical properties of self-healed film, a rectangular EPB film with a length of 50 mm and width of 10 mm was cut and subject to healing at room temperature by 5 min pressing with fingers, and subsequent healing during 1 h. The healed EPB film was able to bear a load of 200 g, similar to the initial film (Fig. 6c).

The electrical conductivity (σ) of EPB films was found from voltampere curves (see Fig. 6b). For the samples before and after the self-healing values σ were the same order of magnitude: 0.63 and 0.40 S·cm^{-1}, respectively. As it is seen in Fig. 6(d), the electroconductivity of the samples after the self-healing was enough to pass sufficient current for illuminating of a LED bulb. The lower conductivity for the sample after self-healing can be connected with voids that can form at the contact area as it will be demonstrated further in SEM images of cross-sections of healed sample.

The values of electrical conductivity achieved in this work is higher than for PVA/PANI composite described in the literature. For example, a PVA/PANI composite crosslinked with boric acid displayed a conductivity of 0.052 S·cm^{-1},[45] while PVA/1-butyl-3-methylimidazolium tetrafluoroborate/ PANI exhibited a conductivity of 0.0639 S·cm^{-1}.[46] Furthermore, our results are comparable to other materials based on graft PANI copolymers. For example, poly(styrenesulfonic acid-*g*-PANI) demonstrated a conductivity up to 0.149 S·cm^{-1},[47] and poly(vinyl chloride)-*g*-PANI with 0.73 S·cm^{-1}.[48]

For deeper discussion of influence of ambient humidity on self-healing, the water sorption isotherms of EPB samples were measured and analyzed using the Laatikainen-Lindström quasi-chemical sorption model. The detailed description of model is given in ESI. Experimental sorption data and results of its approximation are given in Fig. 7(a) as points and lines, respectively. According to selected model the overall sorption can be divided into sorption on active sites (polar groups of polymers) and sorption in clusters (sorption on previously sorbed water molecules accompanied with swelling of polymer matrix) using refined parameters as it is described in ESI. The corresponding curves are given in Fig. 7 as dashed (sorption) and dotted (sorption in clusters) lines, respectively. It should be noted that the self-healing process proceeds via the interaction of polar groups of polymers and depends on the mobility of polymer chains in the material, which is necessary for the implementation of intermolecular contact between polar groups. The presented results show that the saturation of the active sorption sites of the polymer does not occur. This suggests that the polar groups of the copolymer, such as the dopant ions in PANI, as well as the amide and hydroxyl groups of PAAm and PVA, are not fully accessible for sorbate binding. It can be proposed that hydrophobic PANI chains are exposured to the surface of the film and this re-

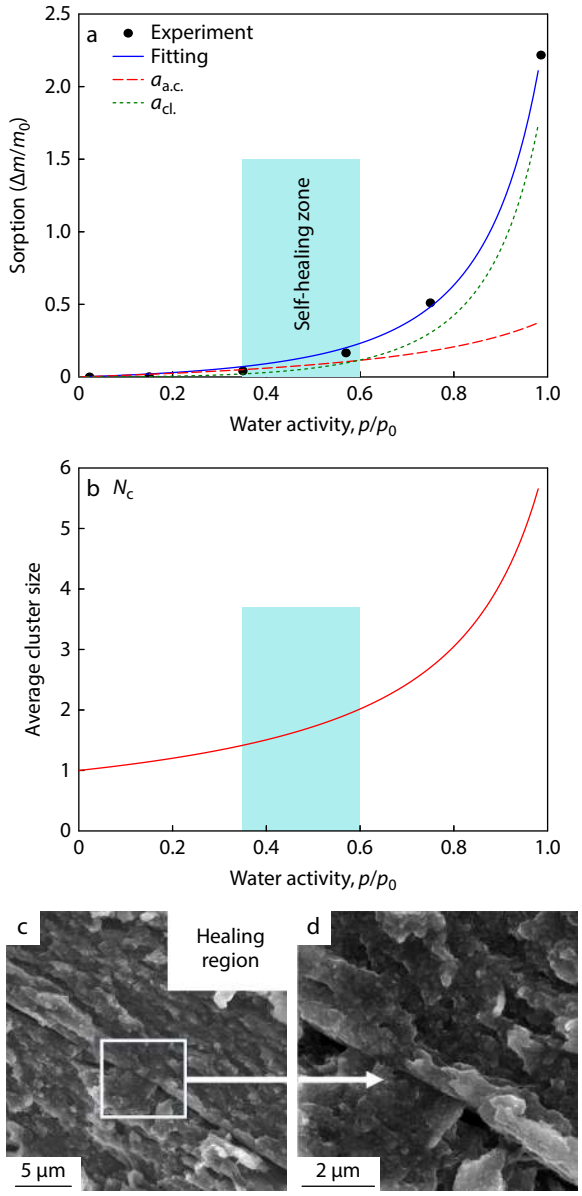

Fig. 7 Isotherm of water sorption by EPB sample (a), the experimental (dots) filling with Laatikainen-Lindström equation (solid line), sorption of water on active sites (dushed line), in clusters (dotted line); average number of water molecules in sorption cluster (b) and cross-section of film after self-healing at different magnifications (c, d).

https://doi.org/10.1007/s10118-024-3113-9

sults in poor self-healing at low RH values. An increase in sorption on active sites with growth of p/p_0 is associated with an increase in their availability due to polymer swelling and rising of their accessibility for interactions between each other thus improving the self-healing. Further it can be proposed, that at RH>60% the polar polymer groups become surrounded with high amount of water due to sorption in clusters that again reduces the possibility of their interaction between each other that complicates the self-healing process more difficult. Thus, it can be concluded that optimal water content for self-healing of electroconducting film is needed to maintain the accessibility of active cites (polar groups) and mobility of polymer chains. At RH≤35%, sorption in clusters, which is associated with polymer swelling and, therefore, with an increase in the mobility of polymer chains, does not yet occur. Growth of RH higher than 60% results in superiority of sorption in clusters over sorption on active cites that also not preferable for self-healing. The Eq. S4 (in ESI), gives possibility to estimate the dependence of size of water clusters (N_c) in a material on the humidity level (see Fig. 7b). The optimal average cluster size at which the process of its self-healing proceeds effectively as N_c=1.9 that means that in already 2 water molecules per binding site prevents effective self-healing.

The cross-section of self-healed area was investigated using the scanning electron microscopy (Figs. 7c and 7d). The EPB film after self-healing at RH=57% was frozen in liquid nitrogen and cleaved in self-healing region. The surface of the cleaved films is folded, that characterizes the presence of structural inhomogeneities in the bulk of the material and is most likely associated with the formation of regions enriched with conducting polymer chains (network of electroconducting pathways). Additionally, the given cross-section shows the formation of area of coalescence of the surface of the films in the contact region (Fig. 7d). The coalescence does not cover all contact region (voids are visible on the cross section in contact area) but its amount at optimal conditions is sufficient to restore the mechanical characteristics and most part of electrical conductivity of EPB films after the self-healing process.

Supercapacitor Performance

A physical diagram of the assembled two-electrode supercapacitor device based on EPB electrodes and the results of investigation of its electrochemical performance are shown in Fig. 8. The Nyquist plot is presented in Fig. 8(b). A semi-circle with low diameter (<0.3 Ω) at a high frequency range region (see inset to the Fig. 8b) is observed indicating a low charge transfer resistance at the electrode/gel electrolyte interface, while a quite short part with 45° slope attributed to Warburg impedance im-

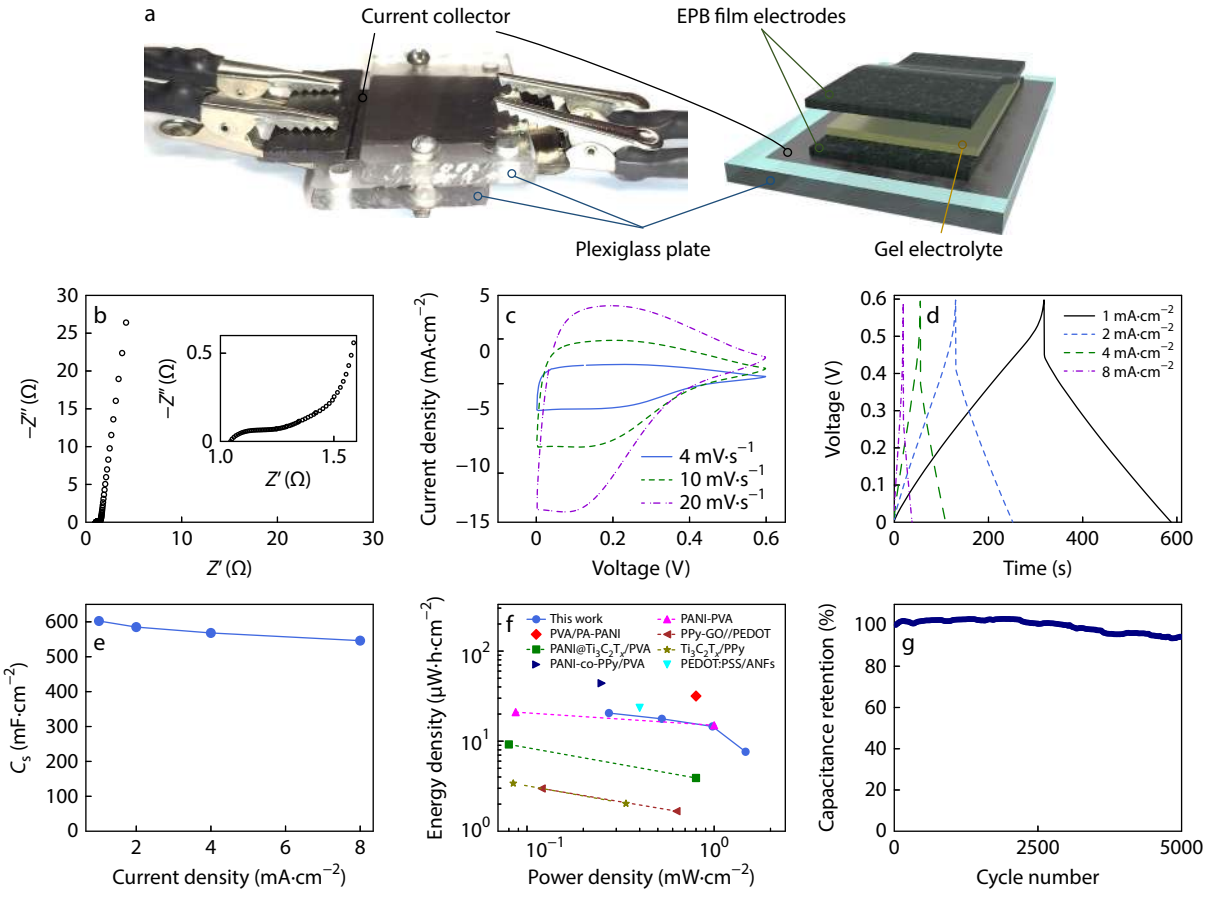

Fig. 8 A physical diagram of the two-electrode supercapacitor cell (a), the Nyquist plot for two-electrode supercapacitor (b) (inset is the magnified view in high frequency range region), CVA curves at scan rates of 4, 10 and 20 mV·s^{-1} (c), GCD curves at current densities of 1–8 mA·cm^{-2} (d), specific capacitance versus current density (e), Ragone plot (f), cycling performance (g).

https://doi.org/10.1007/s10118-024-3113-9

plying fast diffusion of electrolyte ions into electrode.[49] At the same time, low-frequency region $-Z''(Z')$ dependence has a slope of ~84° that is close to vertical line ascribed to ideal capacitive behavior. A slight deviation from ideal capacitor can be caused by inhomogeneity of surface geometry (roughness) and chemical structure (Faradic active sites of PANI) of the electrode material.[50]

The oxidative-reduction peaks symmetrically arranged at 0.1–0.2 V are clearly seen on a CVA curves at various scan rates (Fig. 8c) implying a rapid kinetic of the redox transitions of PANI chains. The deviation of the CVA curve from rectangular shape with pronounced peaks may be related to large contribution of pseudocapacitance for charge storage. The typical GCD curves presented in Fig. 8(d) demonstrate nearly triangular shape that confirms rapid redox reactions. The specific capacitance (C_s) calculated based on the GCD curves reached 602 mF·cm^{-2} at the current density of 1 mA·cm^{-2} (75 F/g at 0.13 A·g^{-1}) and remained 546 mF·cm^{-2} at 8 mA·cm^{-2} (Fig. 8d) due to fast redox kinetics. The obtained capacitance of the cell in this work is higher compared with others recently reported PANI-based charge storage devices, such as, supercapacitors (SC) with electrodes based on a double-cross-linked PANI-PVA (237 mF·cm^{-2} at 0.5 mA·cm^{-2}),[51] PANI@$Ti_3C_2T_x$/PVA composite (103.8 mF·cm^{-2} at 2 mA·cm^{-2}),[52] PVA/phytic acid-PANI (356 mF·cm^{-2} at 1 mA·cm^{-2})[53] and PANI-*co*-polypyrrole(PPy)/PVA (317 mF·cm^{-2} at 1 mA·cm^{-2}).[54] The maximum calculated areal energy and power densities for assembled SC reached 20.5 μW·h·cm^{-2} and 1.5 mW·cm^{-2}. The relationships between E_s and P_s calculated at varied current density are illustrated on a Ragone plot in Fig. 8(f) and compared to other reported SC,[51,52] PPy-graphene oxide/poly(3,4-ethylenedioxythiophene) (PPy-GO/PEDOT),[55] $Ti_3C_2T_x$/PPy[56] and PEDOT:polystyrene sulfonate/aramid nanofiber (PEDOT:PSS/ANFs).[57] The capacitance retention ratio was 94% after applying of 5000 charge-discharge cycles at the current density of 2 mA·cm^{-2} (Fig. 8g), that is higher than for SC with PANI/carboxylated chitosan-PVA electrodes (78% after 500 GCD cycles)[58] and higher than PEDOT:PSS/ANFs-based SC (67% after 1000 cycles).[57] Thus, the performance of PVA-PAAm-PANI-based SC was the same order of magnitude and in some cases even higher than that for different conductive polymer electrode-based cells (PANI, PPy and PEDOT).

CONCLUSIONS

In summary, the work demonstrated the successful synthesis of water-soluble ternary graft copolymer consisting of poly(vinyl alcohol) (PVA), polyacrylamide (PAAm) and poly(aniline-*co*-*p*-phenylenediamine) (PAPhDA), which showed promising potential for producing of electroactive self-healing films. The use of atomic force microscopy revealed that the PVA-PAAm-PAPhDA polymer brush exhibited a more uniform distribution of conducting pathways on the surface compared to PVA-PAPhDA and PAAm-PAPhDA. This observation may be attributed to the different functions of PVA as a stabilizer for PAPhDA and PAAm as a backbone for growing PAPhDA chains. Furthermore, the optimal PVA/PAAm ratio in the polymer brush was found to enhance its electrochemical activity, presumably due to its highest compatibility with water. Notably, the self-healing process resulted in the significant restoration of both mechanical and electrical characteristics of the material. Scanning electron microscopy study confirms the presence of fused areas at the point of contact during the self-healing process, which effectively occurred at a relative humidity of 57%. The analysis of the sorption data suggests that the presence of the optimal level of water vapor activity is associated with optimal balance between the plasticizing effect of water and the shielding of the polar centers of the polymer by clusters of water molecules. The successful application of PVA-PAAm-PAPhDA-based films as flexible two-electrode supercapacitor was demonstrated. The constructed supercapacitor cell demonstrated a high specific capacitance of 602 mF·cm^{-2} and good cycling stability with a capacitance retention of 94% after 5000 cycles.

Conflict of Interests

The authors declare no interest conflict.

Electronic Supplementary Information

Electronic supplementary information (ESI) is available free of charge in the online version of this article at http://doi.org/10.1007/s10118-024-3113-9.

Data Availability Statement

The data that support the findings of this study are available from the corresponding author upon reasonable request. The authors' contact information: pmarip@mail.ru (S.M.P.), smirnov_michael@mail.ru (S.M.A.).

ACKNOWLEDGMENTS

The work was carried out within the state assignment №124013000728-0. The experimental work was also in part facilitated with equipment of the Engineering Center of St. Petersburg State Technological Institute (Technical University).

REFERENCES

1 Yang, L; Xin, Z; Biporjoy, S; Noémy, G. L; Fabio, C. Recent progress on self-healable conducting polymers. *Adv. Mater.* **2022**, *34*, 2108932.
2 Arvas, M.B.; Yazar, S.; Sahin, Y. Electrochemical synthesis and characterization of self-doped aniline 2-sulfonic acid-modified flexible electrode with high areal capacitance and rate capability for supercapacitors. *Synth. Met.* **2022**, *285*, 117017.
3 Hou, X.; Zhou, Y.; Liu, Y.; Wang, L.; Wang, J. Coaxial electrospun flexible PANI//PU fibers as highly sensitive pH wearable sensor. *J. Mater. Sci.* **2020**, *55*, 16033–16047.
4 Sofyan, N.; Nugraha, R.A.; Ridhova, A.; Yuwono, A.H.; Udhiarto, A. Characteristics of PANi/rGO nanocomposite as protective coating and catalyst in dye-sensitized solar cell counter electrode deposited on AISI 1086 steel substrate. *Int. J. Eng.* **2018**, *31*, 1741–1748.
5 Shahabuddin, S.; Gaur, R.; Mukherjee, N.; Chandra, P.; Khanam, R. Conducting polymers-based nanocomposites: innovative materials for waste water treatment and energy storage. *Mater.*

Today Proc. **2022**, *62*, 6950–6955.
6 Abdel Rehim, M. H.; Yassin, M. A.; Zahran, H.; Kamel, S.; Moharam, M. E.; Turky, G. Rational design of active packaging films based on polyaniline-coated polymethyl methacrylate/nanocellulose composites. *Polym. Bull.* **2020**, *77*, 2485–2499.
7 Guarino, V.; Alvarez-Perez, M.A.; Borriello, A.; Napolitano, T.; Ambrosio, L. Conductive PANi/PEGDA macroporous hydrogels for nerve regeneration. *Adv. Healthc. Mater.* **2013**, *2*, 218–227.
8 Ghosh, S.; Roy, S. Nonlinear analysis of a fiber-reinforced tubular conducting polymer-based soft actuator. **2022**.
9 Farooq, A. S.; Zhang, P. A comprehensive review on the prospects of next-generation wearable electronics for individualized health monitoring, assistive robotics, and communication. *Sens. Actuators A Phys.* **2022**, *344*, 113715.
10 Vorobiov, V. K.; Smirnov, M. A.; Bobrova, N. V.; Sokolova, M. P. Chitosan-supported deep eutectic solvent as bio-based electrolyte for flexible supercapacitor. *Mater. Lett.* **2021**, *283*, 128889.
11 Zhang, C.; Chen, Z.; Rao, W.; Fan, L.; Xia, Z.; Xu, W.; Xu, J. A high-performance all-solid-state yarn supercapacitor based on polypyrrole-coated stainless steel/cotton blended yarns. *Cellulose* **2019**, *26*, 1169–1181.
12 Batishcheva, E. V; Smirnov, N. N.; Bobrova, N. V; Sokolova, M. P.; Smirnov, M. A. Ion-conducting membranes based on bacterial cellulose nanofibers modified by poly(sodium acrylate-*co*-2-acrylamido-2-methylpropanesulfonic acid). *Chinese J. Polym. Sci.* **2023**, *42*, 1–11.
13 Sidheekha, M.P.; Rajan, L.; Ismail, Y.A. Reaction driven biomimetic sensing characteristics of polyaniline/chitosan hybrid film: sensing chemical and electrical reaction conditions. *Mater. Chem. Phys.* **2022**, *279*, 125769.
14 Smirnov, M. A.; Sokolova, M. P.; Geydt, P.; Smirnov, N. N.; Bobrova, N. V.; Toikka, A. M.; Lahderanta, E. Dual doped electroactive hydrogelic fibrous mat with high areal capacitance. *Mater Lett.* **2017**, *199*, 192–195.
15 Riaz, U.; Singh, N.; Rashnas Srambikal, F.; Fatima, S. A review on synthesis and applications of polyaniline and polypyrrole hydrogels. *Polym. Bull.* **2023**, *80*, 1085–1116.
16 Upadhyay, J.; Das, T. M.; Borah, R.; Paul, K.; Acharjya, K. Ternary nanocomposites of rGO:RuO_2:Pani based flexible electrode for supercapacitor applications. *Solid State Commun*. **2021**, *334–335*, 114382.
17 Smirnov, M.A.; Tarasova, E. V.; Vorobiov, V.K.; Kasatkin, I.A.; Mikli, V.; Sokolova, M.P.; Bobrova, N. V.; Vassiljeva, V.; Krumme, A.; Yakimanskiy, A. V. Electroconductive fibrous mat prepared by electrospinning of polyacrylamide-*g*-polyaniline copolymers as electrode material for supercapacitors. *J. Mater. Sci.* **2019**, *54*, 4859–4873.
18 Bavatharani, C.; Muthusankar, E.; Wabaidur, S. M.; Alothman, Z. A.; Alsheetan, K. M.; AL-Anazy, M. M.; Ragupathy, D. Electrospinning technique for production of polyaniline nanocomposites/nanofibres for multi-functional applications: a review. *Synth. Met.* **2021**, *271*, 116609.
19 Smirnov, M. A.; Sokolova, M. P.; Bobrova, N. V.; Toikka, A. M.; Morganti, P.; Lahderanta, E. Synergistic effect of chitin nanofibers and polyacrylamide on electrochemical performance of their ternary composite with polypyrrole. *J. Energy Chem.* **2018**, *27*, 843–853.
20 Pyarasani, R. D.; Jayaramudu, T.; John, A. Polyaniline-based conducting hydrogels. *J. Mater. Sci.* **2019**, *54*, 974–996.
21 Zhang, L.; Li, T.; Yu, Y.; Shi, K.; Bei, Z.; Qian, Y.; Qian, Z. An injectable conductive hydrogel restores electrical transmission at myocardial infarct site to preserve cardiac function and enhance repair. *Bioact. Mater.* **2023**, *20*, 339–354.
22 Elyashevich, G. K.; Sidorovich, A. V.; Smirnov, M. A.; Kuryndin, I. S.; Bobrova, N. V.; Trchová, M.; Stejskal, J. Thermal and structural stability of composite systems based on polyaniline deposited on porous polyethylene films. *Polym. Degrad. Stabil.* **2006**, *91*, 2786–2792.
23 Elyashevich, G.K.; Smirnov, M.A.; Kuryndin, I.S.; Bukošek, V. Electroactive composite systems containing high conductive polymer layers on poly(ethylene) porous films. *Polym. Adv. Technol.* **2006**, *17*, 700–704.
24 Maity, N.; Dawn, A. Conducting polymer grafting: recent and key developments. *Polymers* **2020**, *12*, 709.
25 Isakova, A. A.; Gribkova, O. L.; Aliev, A. D.; Indenbom, A. V.; Shevlyakova, N. V.; Tverskoi, V. A.; Nekrasov, A. A. The synthesis of polyaniline in polyethylene films with grafted sulfonated polystyrene and properties of these films. *Prot. Metals Phys. Chem. Surf.* **2020**, *56*, 725–733.
26 Mostafaee, H.; Moghadam, P. N.; Khalafy, J. Improvement of polyaniline processability by graft reaction of polyaniline on poly(glycidyl methacrylate-*alt*-maleic anhydride) copolymer: synthesis and characterization. *Polym. Sci. Ser. B* **2019**, *61*, 827–834.
27 Xiang, Q.; Xie, H. Q. Preparation and characterization of alkali soluble polyacrylamide-g-polyaniline. *Eur. Polym. J.* **1996**, *32*, 865–868.
28 Shen, Z.; Zhang, Z.; Zhang, N.; Li, J.; Zhou, P.; Hu, F.; Rong, Y.; Lu, B.; Gu, G. High-stretchability, ultralow-hysteresis conducting polymer hydrogel strain sensors for soft machines. *Adv. Mater.* **2022**, *33*, 2203650.
29 Abdelhamied, M. M.; Abdelreheem, A. M.; Atta, A. Influence of ion beam and silver nanoparticles on dielectric properties of flexible PVA/PANI polymer composite films. *Plastics, Rubber and Compos.* **2022**, *51*, 1–12.
30 Akram, D.; Hameed, N. Preparation and characterization of PANI/PVA blends as electrolyte materials. *J. Appl. Sci. Nanotechnol.* **2022**, *2*, 38–46.
31 Xie, Z.; Hu, B.L.; Li, R.W.; Zhang, Q. Hydrogen bonding in self-healing elastomers. *ACS Omega* **2021**, *6*, 9319–9333.
32 Smirnov, M. A.; Nikolaeva, A. L.; Bobrova, N. V.; Vorobiov, V. K.; Smirnov, A. V.; Lahderanta, E.; Sokolova, M. P. Self-healing films based on chitosan containing citric acid/choline chloride deep eutectic solvent. *Polym. Test.* **2021**, *97*, 107156.
33 Liu, Y.; Mao, J.; Guo, Z.; Hu, Y.; Wang, S. Polyvinyl alcohol/carboxymethyl chitosan hydrogel loaded with silver nanoparticles exhibited antibacterial and self-healing properties. *Int. J. Biol. Macromol.* **2022**, *220*, 211–222.
34 Gaylord, N. Proposed new mechanism for catalyzed and uncatalyzed graft polymerization onto cellulose. *J. Polym. Sci., Part C: Polym. Symp.* **1972**, *172*, 153–172.
35 Smirnov, M. A.; Sokolova, M. P.; Bobrova, N. V.; Kasatkin, I. A.; Lahderanta, E.; Elyashevich, G. K. Capacitance properties and structure of electroconducting hydrogels based on copoly(aniline-P-phenylenediamine) and polyacrylamide. *J. Power Sources* **2016**, *304*, 102–110.
36 Sokolova, M. P.; Smirnov, M. A.; Samarov, A. A.; Bobrova, N. V; Vorobiov, V. K.; Popova, E. N.; Filippova, E.; Geydt, P.; Lahderanta, E.; Toikka, A. M. Plasticizing of chitosan films with deep eutectic mixture of malonic acid and choline chloride. *Carbohydr. Polym.* **2018**, *197*, 548–557.
37 Lai, S.; Casu, M.; Saba, G.; Lai, A.; Husu, I.; Masci, G.; Crescenzi, V. Solid-state ^{13}C NMR study of poly(vinyl alcohol) gels. *Solid State Nucl. Magn. Reson.* **2002**, *21*, 187–196.
38 Mjakin, S. V.; Sychov, M.M.; Sheiko, N.B.; Ezhenkova, L.L.; Rodionov, A.G.; Vasiljeva, I. V. Improvement of vibrodamping properties of polyvinyl acetate-graphite composites by electron beam processing of the filler. *Springerplus* **2016**, *5*, 1539.
39 Tarasova, N.; Zanin, A.; Krivoborodov, E.; Toropygin, I.; Pascal, E.; Mezhuev, Y. The New Approach to the preparation of polyacrylamide-based hydrogels: initiation of polymerization of acrylamide with 1,3-dimethylimidazolium (phosphonooxy-)oligosulphanide under drying aqueous solutions. *Polymers*

2021, *13*, 1806.
40 Goswami, S.; Nandy, S.; Calmeiro, T.R.; Igreja, R.; Martins, R.; Fortunato, E. Stress induced mechano-electrical writing-reading of polymer film powered by contact electrification mechanism. *Sci. Rep.* **2016**, *6*, 19514.
41 Potje-Kamloth, K; Polk, B. J; Josowicz, M; Janata, L. Doping of polyaniline in the solid state with photogenerated triflic acid. *Chem. Mater.* **2002**, *14*, 2782−2787.
42 Khalil, H.; Levon, K. Shear-induced delocalization of polarons in polyaniline-surfactant complexes. *Macromolecules* **2002**, *35*, 8180−8184.
43 Trchová, M.; Šeděnková, I.; Konyushenko, E.N.; Stejskal, J.; Holler, P.; Ćirić-Marjanović, G. Evolution of polyaniline nanotubes: the oxidation of aniline in water. *J. Phys. Chem. B* **2006**, *110*, 9461−9468.
44 Li, Y.; Bober, P.; Trchová, M.; Stejskal, J. Colloidal dispersions of conducting copolymers of aniline and p-phenylenediamine for films with enhanced conductometric sensitivity to temperature. *J. Mater. Chem. C* **2017**, *5*, 1668−1674.
45 Xue, H.; Mi, Z.; Shi, L.; Yang, X.; Chen, R.; Luo, X.; Guan, Y. A high-toughness, tailorable, wearable multifunctional sensor based on multisynergistic fabric-hydrogel constructed *via* dual-function boric acid bridge. *Mater. Today Chem.* **2023**, *33*, 101696.
46 Du, H.; Wang, J.; Wu, Z.; Liu, Z. Polyaniline grown on poly(vinyl alcohol)/ionic liquid composite film as electrodes for flexible and self-healable solid-state polymer supercapacitors. *Polymer* **2022**, *255*, 125129.
47 Lee, J. W.; Lee, J. U.; Jo, J. W.; Bae, S.; Kim, K. T.; Jo, W. H. In-situ preparation of graphene/poly(styrenesulfonic acid-graft-polyaniline) nanocomposite via direct exfoliation of graphite for supercapacitor application. *Carbon* **2016**, *105*, 191−198.
48 Massoumi, B.; Mohammad-Rezaei, R.; Jaymand, M. Chemical and electrochemical grafting of polyaniline onto poly(vinyl chloride): synthesis, characterization, and materials properties. *Polym. Adv. Technol.* **2016**, *27*, 1056−1063.
49 Eftekhari, A. Surface diffusion and adsorption in supercapacitors. *ACS Sustainable Chem. Eng.* **2019**, *7*, 3692−3701.
50 Córdoba-Torres, P.; Mesquita, T. J.; Nogueira, R. P. Relationship between the origin of constant-phase element behavior in electrochemical impedance spectroscopy and electrode surface structure. *J. Phys. Chem. C* **2015**, *119*, 4136−4147.
51 Zhao, J.; Cao, L.; Lai, F.; Wang, X.; Huang, S.; Du, X.; Li, W.; Lin, Z.; Zhang, P. Double-cross-linked polyaniline hydrogel and its application in supercapacitors. *Ionics* **2022**, *28*, 423−432.
52 Cao, S.; Zhao, T.; Li, Y.; Yang, L.; Ahmad, A.; Jiang, T.; Shu, Y.; Jing, Z.; Luo, H.; Lu, X.; Zhang, H. Fabrication of PANI@$Ti_3C_2T_x$/PVA hydrogel composite as flexible supercapacitor electrode with good electrochemical performance. *Ceram. Int.* **2022**, *48*, 15721−15728.
53 Gao, X.; Hu, Q.; Sun, K.; Peng, H.; Xie, X.; Hamouda, H.A.; Ma, G. A novel all-in-one integrated flexible supercapacitor based on self-healing hydrogel electrolyte. *J. Alloys Compd.* **2021**, *888*, 161554.
54 Tao, X. Y.; Wang, Y.; Ma, W.; Ye, S. F.; Zhu, K. H.; Guo, L. T.; Fan, H. L.; Liu, Z. S.; Zhu, Y. B.; Wei, X. Y. Copolymer hydrogel as self-standing electrode for high performance all-hydrogel-state supercapacitor. *J. Mater. Sci.* **2021**, *56*, 16028−16043.
55 Wang, N.; Wang, X.; Zhang, Y.; Hou, W.; Chang, Y.; Song, H.; Zhao, Y.; Han, G. All-in-one flexible asymmetric supercapacitor based on composite of polypyrrole-graphene oxide and poly(3,4-ethylenedioxythiophene). *J. Alloys Compd.* **2020**, *835*, 155299.
56 Zhang, C.; Xu, S.; Cai, D.; Cao, J.; Wang, L.; Han, W. Planar supercapacitor with high areal capacitance based on Ti_3C_2/Polypyrrole composite film. *Electrochim. Acta.* **2020**, *330*, 135277.
57 Liu, G.; Zheng, L.; Sun, Y.; Zhang, M.; Xiong, C. Preparation of flexible conductive composite electrode film of PEDOT:PSS/Aramid nanofibers *via* vacuum-assisted filtration and acid post-treatment for efficient solid-state supercapacitor. *Int. J. Hydrogen Energy* **2022**, *47*, 22454−22468.
58 Yu, M.; Ji, X.; Ran, F. Chemically building interpenetrating polymeric networks of Bi-crosslinked hydrogel macromolecules for membrane supercapacitors. *Carbohydr. Polym.* **2021**, *255*, 117346.

https://doi.org/10.1007/s10118-024-3113-9